Genes & Diseases (2023) 10, 284–300

Available online at www.sciencedirect.com

ScienceDirect

journal homepage: www.keaipublishing.com/en/journals/genes-diseases

FULL LENGTH ARTICLE

Liquiritigenin promotes osteogenic differentiation and prevents bone loss via inducing auto-lysosomal degradation and inhibiting apoptosis

Yu Qiu [a,b,1], Yueyang Zhao [b,c,1], Zhimin Long [b,c], Aijia Song [d], Peng Huang [d], Kejian Wang [b,c], Ling Xu [a,], David Paul Molloy [e,***], Guiqiong He [b,c,*]**

[a] *College of Stomatology, Chongqing Medical University, Chongqing Key Laboratory of Oral Diseases and Biomedical Sciences, Chongqing Municipal Key Laboratory of Oral Biomedical Engineering of Higher Education, Chongqing 400016, China*
[b] *Chongqing Key Laboratory of Neurobiology, Chongqing Medical University, Chongqing 400016, China*
[c] *Department of Anatomy, Chongqing Medical University, Chongqing 400016, China*
[d] *Laboratory of Medical Experiment Technology, Institute of Life Science, Chongqing Medical University, Chongqing 400016, China*
[e] *Department of Biochemistry and Molecular Biology, Chongqing Medical University, Chongqing 400016, China*

Received 16 January 2021; received in revised form 16 June 2021; accepted 22 June 2021
Available online 13 July 2021

KEYWORDS
Apoptosis;
Auto-lysosomal degradation;
Liquiritigenin;
Osteogenic differentiation;

Abstract Osteoporosis (OP) is a debilitating skeletal abnormality involving bone remodeling and bone cell homeostasis characterized by decreased bone strength and high fracture risk. A novel therapeutic intervention for OP by manipulating cellular autophagy–apoptosis processes to promote skeletal homeostasis is presented. Protective effects of the naturally occurring plant extract Liquiritigenin (LG) were demonstrated in an ovariectomy (OVX)-OP mouse model and preosteoblast MC3T3-E1 cells. Micro-CT and histological staining assessments of skeletal phenotype were applied alongside detection of autophagy activity in osteocytes and MC3T3-

* Corresponding author. Chongqing Key Laboratory of Neurobiology, Chongqing Medical University, No.1 Yixueyuan Road, Yuzhong District, Chongqing 400016, China. Fax: +86(0)23 89129930.
** Corresponding author. Department of Prosthodontics, Stomatological Hospital of Chongqing Medical University, 426# Songshibei Road, Yubei District, Chongqing 401147, China. Fax: +86(0)23 89035858.
*** Corresponding author. Department of Biochemistry and Molecular Biology, Chongqing Medical University, No.1 Yixueyuan Road, Yuzhong District, Chongqing 400016, China. Fax: +86(0)23 68485111.
E-mail addresses: 500203@hospital.cqmu.edu.cn (L. Xu), 190495@cqmu.edu.cn (D.P. Molloy), guiqionghe@cqmu.edu.cn (G. He).
Peer review under responsibility of Chongqing Medical University.
[1] These authors contributed equally to this work.

https://doi.org/10.1016/j.gendis.2021.06.008

Osteoporosis

E1 cells by transmission electron microscopy (TEM). The effects of LG on chloroquine (CQ)- and the apoptosis-inducing TS-treated osteogenic differentiations and status of lysosomes within MC3T3-E1 cells were analyzed by Neutral red, Alizarin red S and alkaline phosphatase (ALP) staining and Western blot assays. Treatment with LG prevented bone loss, increased osteogenic differentiation *in vivo* and *in vitro*, and inhibited osteoclast formation to some extent. TEM analyses revealed that LG can improve auto-lysosomal degradation within osteocytes from OVX mice and MC3T3-E1 cells. The abnormal status of lysosomes associated with CQ and TS treatments was notably alleviated by LG which also reduced levels of apoptosis-induced inhibition of osteogenic differentiation and averted abnormal osteogenic differentiation as a consequence of a blockage in autolysosome degradation. Overall, LG stimulates bone growth in OVX mice through increased osteogenic differentiation and regulation of autophagy-apoptosis mechanisms, presenting an auspicious natural therapy for OP.

Introduction

Osteoporosis (OP) is an enervating systemic bone disorder manifested by low bone mass. As a repercussion of faulty intracellular degradation processes that deplete bone ultrastructure, the disorder culminates in an increased risk of skeletal fragility and fracture.[1,2] This degenerative condition afflicts millions of people worldwide, being prevalent amongst adult females with one in three sufferers, most notably post-menopausal women, alongside one in five men. In essence, OP gives rise to an enormous economic and emotional familial burden.[3,4] Amongst the numerous primary strategies presently available for the alleviation of OP, estrogen replacement therapy, bisphosphonates and selective estrogen receptor modulators are frequently applied. However, many of these also impose unwarranted and detrimental side effects, including mammary cancers and atypical femoral fractures, which delimit their clinical application.[5] Consequently, alternative therapeutic regimens in the treatment of OP are essential.

OP is chronic metabolic osteopathy that arises through impaired intracellular lysosomal functioning to disrupt the equilibrium between the various endogenous bone cells (osteoblasts, osteocytes and osteoclasts).[6–8] Any imbalance of energy, amino acid and mineral bio-recycling, which are otherwise prerequisites for cellular viability and organism longevity, will inevitably progress OP.[9,10] Of note, within the lysosomal degradation pathway are branch reactions that involve autophagy. While these can augment bone formation, OP is meliorated through activation of the initial stage of autophagy in the presence of Rapamycin.[11,12] In contrast, osteoblast differentiation and mineralisation are obstructed when autophagy is inhibited.[13] Significant contributions to this can be achieved by, for example, deletion of the Atg5 gene in osteoblasts manifested by a reduction of bone mass *in vivo*, although knockdown of Atg7 and Beclin-1 genes are evinced through impaired osteogenic functionality within certain osteoblastic cell lines.[14] Thus, autophagy is unequivocal for bone homeostasis.[15]

Despite the oversight mentioned above, present contentions for the onset and development of OP notably include asynchronous autophagy inhibition and committed apoptosis at any stage during osteoblast existence.[15–19] Ubiquitous cellular regulators may mediate coeval apoptosis-autophagy workings within osteoblasts, including Bcl-2 and Beclin-1 proteins preeminent in the aetiology of several diseases[17,20,21] with correct modulation of an autophagy-apoptosis equilibrium state throughout expected osteoblast lifespan being innate for bone mass homeostasis.[22]

Historical studies have utilised various naturally occurring plant products as therapeutic agents for and alleviation of bone diseases.[23,24] One such compound, namely Liquiritigenin (LG), a low molecular weight dihydroflavonoid extract from the *Glycyrrhiza glabra* root, was more recently demonstrated to impart anti-tumour, -oxidative and -inflammatory biological properties.[25] These characteristics would seemingly support the notion that LG could circumvent ROS stress and damage within osteoblasts through, for example, activation of PI3K signalling cascades, alongside up-regulation of mitochondrial activities deemed of importance during oncogenic, oxidative and foment responses.[26,27] Besides, LG treatment may, by shunting osteoclast differentiation into suppression via the TGF-b Smad1/5-dependent pathway and thus devolving bone-resorption through inhibition of NF-kB ligand (RANKL)-induced signalling, promote osteoblastic differentiation.[28]

Whilst an anti-OP activity directly attributable to LG treatment for averting bone loss *in vivo* remains uncertain, insights into the molecular mechanism of LG as a deregulator of apoptosis to de-concatenate several diseases,[29–32] is the central theme of this present work. The evidence presented in this current work indicates that the equilibrium between autophagy and apoptosis within osteoblasts can be manipulated to promote bone formation in an OP-mice model. These data significantly enlighten biophysical events during bone formation as applied to the treatment of OP.

Material and methods

Chemicals and reagents

LG (chemical formula: $C_{15}H_{12}O_4$, molecular weight: 256.2, purity $\geq$ 98%) was obtained from Must Bio-Technology Co. Ltd (Chengdu, China). LG was prepared as a colloid suspension in 0.5% sodium carboxymethylcellulose (CMC; Sangon Biotech, Shanghai, China) for oral treatment of mice.

For cell assays, LG was initially dissolved in DMSO and diluted with 90% α-Minimum Essential Medium (α-MEM, Thermo Fisher Scientific, USA) and 10% Fetal bovine serum (FBS, Biological Industries, USA) to achieve application concentrations. MTT Kit, Trypsin—EDTA Solution, penicillin and streptomycin, BCIP/NBT Alkaline Phosphatase (ALP) Colour Development Kit, Alkaline Phosphatase Assay Kit, Apoptosis Inducer Kit (TNF-α+SM-164, TS) and Neutral red Stain were obtained from Beyotime Biotechnology Co. Ltd (Shanghai, China). Alizarin red S staining solution, 4% paraformaldehyde, hematoxylin and eosin (HE) were purchased from Solarbio Science & Technology Co. Ltd (Beijing, China). Chloroquine (CQ; Sigma) was dissolved in PBS (pH 7.4) to make a 50 mM stock solution.

Animals

Seven-week-old female C57 mice (specific-pathogen-free grade) purchased from the Laboratory Animal Center of Chongqing Medical University were maintained under standard conditions (relative humidity = 50%—60%; ambient temperature = 20 ± 2 °C; 12 h light/dark cycle) with free access to water and food. All animal experiments were approved by the Animal Protection and Ethics Committee of Chongqing Medical University and performed in accordance with the guidelines of laboratory animal care and use.

Experiment design

After a one-week acclimation period, twenty-four 8-week-old female mice were randomly sub-divided into three groups ($n = 8$ per cohort) and anesthetised by isoflurane inhalation prior to surgery. The surgical procedure involved either a sham ovariectomy of bilateral incision and closing sutures without removal of the ovaries (Sham; $n = 8$), or ovariectomy of bilateral incision, removal of both ovaries and closing sutures for 16 mice. Of the 16 ovariectomised mice 8 mice received no further treatment (OVX group). One week following the operation, the remaining 8 ovariectomised mice were supplied with 30 $mg^{-1}kg^{-1}day^{-1}$ LG solvent by intragastric administration for a total of 90 days as per our previous study[33] (OVX + LG group). The other two groups were supplied the same volume of a placebo 0.5% CMC daily by oral gavage for the duration of the treatments. At the end of the treatments, mice in each group were weighed and euthanized. The uteri and bilateral femurs were collected for subsequent histological analysis.

Micro-CT bone analysis

The left femurs of the mice ($n = 6$) were fixed in 4% paraformaldehyde and the bone microarchitecture of their distal end was evaluated by micro-CT (Viva CT40, SCANCO Medical, Brüttisellen, Switzerland) at a resolution of 10.5 mm, energy of 70 kV and 114 mA. The region of interest started end of the growth plate and extended for 100 cross-sections. Parameters, including bone volume/tissue volume (BV/TV), trabecular number (Tb.N), trabecular thickness (Tb.Th), and trabecular spacing (Tb.Sp) were analysed by SCANCO analysis software.

HE staining and immunohistochemistry (IHC)

The right femurs ($n = 6$) were collected and fixed in 4% paraformaldehyde for 24 h. The tissue samples were then decalcified, embedded into paraffin and sectioned to 5-μm thickness.

HE Staining assays were performed according to the manufacturer's instructions. The arrangement and quantities of trabeculae were detected under an optical microscope (DMi8, LEICA, Germany).

Immunohistochemical studies were performed on dewaxed and rehydrated tissue samples incubated in 3% H_2O_2 for 20 min at room temperature (RTP) prior to an overnight incubation at 4°C with the primary antibodies against BMP2 (1:100; ab214821; Abcam), osteopontin (OPN; 1:100; bs-0026R; Bioss), and osteocalcin (OC; 1:100; bs-4917R; Bioss)., anti-Osteocalcin Ab (OC; 1:100; bs-4917R; Bioss). Thereafter, the sections were bathed for 5 min in PBS (× 3) and then incubated with goat anti-mouse HRP secondary Ab (CST, USA) for 1 h at RTP. Freshly prepared Diaminobenzidine (DAB) solution was added and sections were counterstained with hematoxylin. Markers were visualized using a BX51 microscope (Olympus, Shinjuko, Japan). Quantitative analyses were performed using Image J (NIH Image J system, Bethesda, MD, USA).

Tartrate-resistant acid phosphatase (TRAP) staining

For TRAP staining, slides were stained using a TRAP staining kit (Sigma—Aldrich, Cat no. 387A-1 KT) according to the manufacturer's protocol. After dehydration and mounting, the stained slides were observed under a DMi8 microscope (LEICA, Germany) and were analyzed by available software (NIH Image J system, Bethesda, MD, USA) referring to the previous guidelines.[34]

Cell culture

MC3T3-E1 cells were kindly donated by Dr. W. Zhou (Affiliated Rehabilitation Hospital of Chongqing Medical University). Cells were cultured in an incubator maintained at 5% CO_2 and 37°C in α-MEM complete culture medium supplemented with 10% FBS, 100 μg/mL streptomycin and 100 U/mL penicillin.

To initiate osteogenic differentiation, MC3T3-E1 cells at 80% confluency were treated with osteogenic-inducing supplements (herein, termed OIS) containing 50 μg/mL ascorbic acid (Sigma, USA), 5 mM β-glycerophosphate (Sigma, USA) and 10 μM dexamethasone (Sigma, USA). Cells were seeded into 6- and 24-well plates at initial numbers of 2×10^5 and 2.1×10^4 per well, respectively. The 6-well cultures were incubated in the presence of OIS for 7 days prior to Western blot analyses. 24-well plates were induced for 3 and 21 days prior to ALP activity assay and staining and Alizarin red S staining, respectively.

Cell viability assay

The effects of LG on MC3T3-E1 cell viability were measured by MTT assay. Briefly, MC3T3-E1 cells were digested with 0.05% Trypsin—EDTA and collected by centrifugation. The cells were then incubated in 96-well flat-bottom plates (1.0×10^4 cells/well) for 24 h. LG was then added to final concentrations of between 0 and 500 μM for 48 h prior to estimation of cell viability in A_{570nm} microplate (Thermo Scientific, USA) assays.

Alkaline phosphatase activity assay and staining

The density of MC3T3-E1 cells seeded into 24-well plates was 2.1×10^4 cells/well. The MC3T3-E1 cells termed 'blank' group were treated with 90% α-MEM and 10% FBS whilst cells within the experimental groups were treated with LG at 0, 0.5, 1, 5 and 10 μM in concentration in the absence or presence of CQ (1:1000) and TS (1:1000) autophagy inhibitors in OIS for 48 h, respectively. Cells were fixed with 4% paraformaldehyde for 30 min and washed with 0.01 M PBS (3 min × 3). ALP staining was achieved at RTP using a BCIP/NBT alkaline phosphatase colour development kit in the dark for 30 min as per the manufacturer's instruction. The absorbance of each group was detected at the 405 nm using a microplate reader.

Neutral Red staining

Drug treatments and density of the cells were quantified by using Neutral Red Staining to highlight lysosomes within MC3T3-E1 cells. Cells were routinely washed twice in 0.01 M PBS after removal of culture medium. Cells were then fully immersed in Neutral red solution 10 min at RTP. Subsequently, cells were washed twice in PBS two times to remove residual Neutral red solution. Stained lysosomes in living cells were observed by light microscopy.

Alizarin Red S staining

Alizarin Red S staining was performed to determine the level of mineralisation 21 days post-osteogenic induction. Drug treatment regimens and MC3T3-E1 cell densities were described as above. MC3T3-E1 cells were washed three times with 0.01 M PBS to remove residual culture medium and fixed in 4% paraformaldehyde. After 30 min, the stationary liquid was decanted and cells were washed thrice with 0.01 M PBS. Cells were then stained with Alizarin Red S for 30 min at RTP after which excess dye was removed by washing with ddH_2O. Extracellular matrix (ECM) mineral-bound stain was observed and photographed with positive mineralised nodule area quantified using Image J (NIH Image J system, Bethesda, MD, USA).

Flow cytometric analysis

MC3T3-E1 cells were incubated in 6-well plates at a density of 10×10^5 cells well^{-1} for 24 h. Different concentrations of LG were added as prescribed in figure legends. Cells were rinsed twice in PBS and harvested. Flow Cytometry studies were performed using a CytoFLEX Flow Cytometer (Beckman Coulter, USA) within the Life Sciences Institute, Chongqing Medical University, and evaluated by Kaluza Analysis (Beckman Coulter, USA).

Transmission electron microscopy (TEM) analysis

The right femur bone cleaned of muscle and other connective tissue was excised from each mouse ($n = 3$). Bone samples were fixed in 2.5% glutaraldehyde for 48 h and decalcified in a microwave prior to TEM analysis. The MC3T3-E1 cells were collected and fixed in 2.5% glutaraldehyde for 4 h. Both cells and bone tissues were dehydrated, embedded, sectioned and stained using routine protocols. The ultrastructure and status of autophagosomes (APs), auto-lysosomes (ALs) and lysosomes within cells and bone samples were determined using a transmission electron microscope (Philips, Amsterdam, Netherlands) and analyzed referring to the guidelines about monitoring autophagy.[35]

Western blot

Cells were routinely lysed with RIPA buffer (Beyotime) supplemented with PMSF (Beyotime). Protein content was determined using the BCA protein assay (Beyotime) to ensure equal loading of total proteins which were fractionated by 12% SDS-PAGE (CWBIO, Beijing, China) prior to electrophoretic transfer to PVDF membranes (Millipore, USA). Membranes were blocked with 5% non-fat milk prior to overnight incubation at 4°C with primary antibodies against BMP2 (ab214821, Abcam, USA), Beclin-1 (ab62557, Abcam, USA), Lamp1 (ab24170, Abcam, USA), SQSTM1/p62 (#5114, CST, USA), Bcl-2 (#2870, CST, USA), Caspase-3 (66,470-2-1G, Proteintech, Wuhan, China), Bax (ab53154, Abcam, USA), GAPDH (AF7021, Affinity, USA). PDVFs were washed with TBST (× 3), and then incubated for 1 h at RTP with HRP-conjugated secondary antibodies (Proteintech, Wuhan, China). Specific proteins were visualized via enhanced chemiluminescence and a molecular imager (Bio-Rad, CA, USA). Image J software (NIH Image J system, Bethesda, MD, USA) was used to quantify the reactive protein bands. All blot experiments were repeated at least three times. GAPDH served as the internal control for normalization.

Statistical analysis

The data represent the mean ± SD (standard deviation) of three experiments each. All analyses were performed using GraphPad Prism 5 software (GraphPad Software, Inc., La Jolla, CA, USA). The differences between two groups were assayed by Student's *t*-test and ANOVA followed by Newman—Keuls test for three or more groups). Differences were considered statistically significant at $^*P < 0.05$, $^{**}P < 0.01$, $^{***}P < 0.001$.

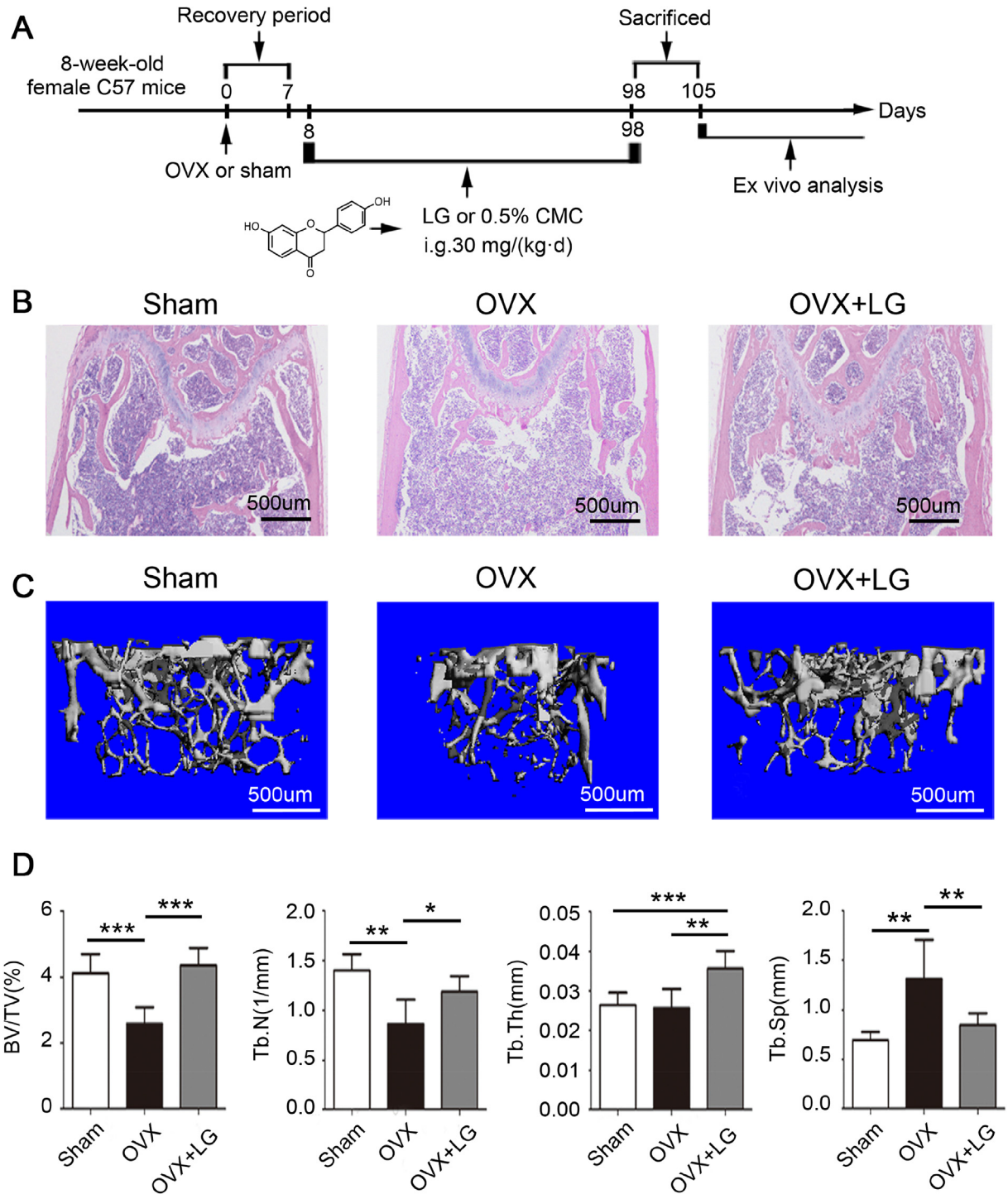

Figure 1 Effect of LG on bone trabecula of mouse femurs in tibia side. Chemical structure of liquiritigenin (LG) and experimental protocol scheme (**A**). HE Staining for mouse femurs in tibia side (**B**) and 3D reconstruction for mouse distal femurs in micro-CT (**C**). Analysis of BV/TV (%), Tb.N (1/mm), Tb.Th (mm) and Tb.Sp (mm) in bone trabecula of mouse femurs in tibia side ($n = 6$) (**D**). Scale bars (B): 500 μm and Scale bars (C): 500 μm. Data are reported as the mean ± standard deviation (SD). *$P < 0.05$, **$P < 0.01$, and ***$P < 0.001$ (one-way analysis of variance/Newman–Keuls test).

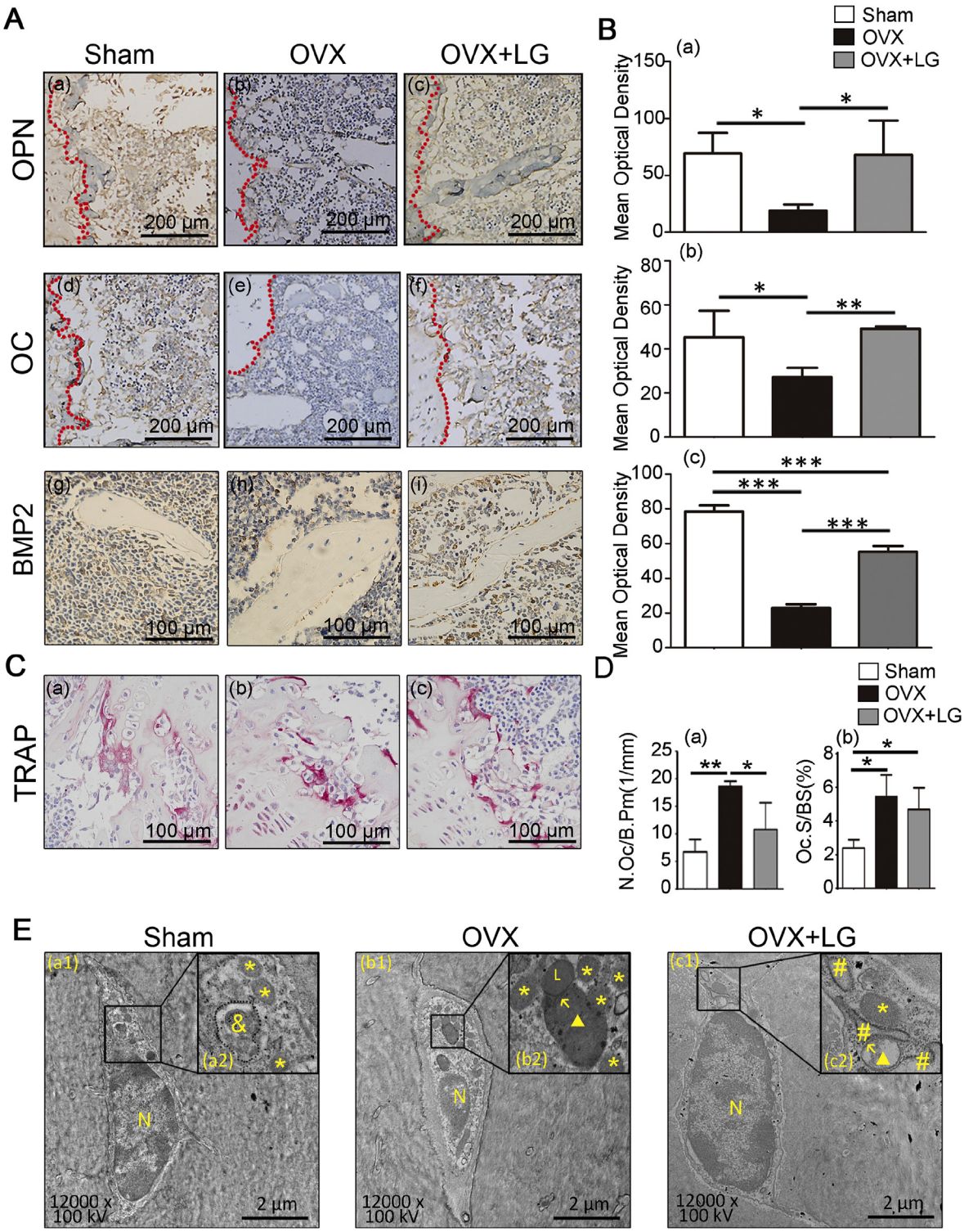

Figure 2 Effect of LG on osteoblasts, osteoclasts, and osteocytes in bone trabecula. The expression of BMP2 OPN, and OC detected by IHC for mouse femurs in tibia side (**A**) and mean optical density of BMP2 OPN, and OC positive cells (**B**). Histological analysis of osteoclasts in different groups via TRAP staining **(C)** and quantitative analysis of the number (N.Oc/B.Pm) and size (Oc.S/BS) of TRAP-positive osteoclasts (**D**). Magnification images of the ultrastructure of osteocytes detected by TEM (**E**). Epiphyseal growth plate outlined by a red dotted line in Aa–f. Cell nucleus (marked as N in **Ea1**–**c1**), AL (outlined by a dotted line in **Ea2**), mitochondria (marked as ***** in **Ea2**–**c2**), APs (marked as ▲ in **Eb2**–**c2**), lysosomes (marked as L in **Eb2**), and developed rough endoplasmic reticula (marked as **#** in **Ec2**) in osteocytes in groups. Scale bars (Ag–i): 100 μm; scale bars (Aa–f and Ca–c): 200 μm; scale bars (E): 2 μm. Data are reported as the mean ± standard deviation (SD) ($n = 3$). *$P < 0.05$, ***$P < 0.001$ (one-way analysis of variance/Newman–Keuls test). N.Oc/B.Pm: osteoclast number/bone perimeter; Oc.S/BS: osteoclast surface/bone surface.

Results

LG militated against bone loss in OVX mice

To analyse regular femur trabeculae architecture in mice models, HE staining was applied and the stained area in OVX mice was significantly larger than that in the Sham mice (Fig. 1A). Interestingly, the converse effects were noted in the presence of LG (Fig. 1B). Micro-CT analyses confirmed that LG lessened bone loss in trabecular compared with that in the OVX group shown by BV/TV, Tb.N, Tb.Th and Tb.Sp (Fig. 1C, D). In all, these data highlight a significant reversal of tissue deterioration within OVX + LG mice.

LG ameliorated bone loss and cellular ultrastructure of bone trabecula within OVX mice

To investigate the biophysical mechanism of LG geared to diminish the destruction of bone tissue in OVX mice, IHC and TRAP histological staining procedures were performed (Fig. 2A–D). Expressions of BMP2, OPN and OC are alleviated in the presence of LG but otherwise obviated as a consequence of ovariectomy (Fig. 2A, B). Second, osteoclast abundance and bone resorption activity in femur tissues were both significantly elevated in OVX mice (Fig. 2Ca-b, D). Interestingly, a decrease in N.Oc/B.Pm was observed in OVX + LG group compared to OVX group, but the Oc.S/BS was comparable across OVX and OVX + LG groups (Fig. 2C, D).

The cellular ultrastructure was also compared between samples from three groups in TEM assays (Fig. 2E). ALs were detected in osteocytes within the Sham group (Fig. 2Ea1-2); however, a large population of dark grey stained bimembranous late-APs was seen to accumulate postoperatively within the cytoplasm of femur tissue cells of OVX-mice (Fig. 2Eb1-2). Furthermore, in osteocytes, monomembranous lysosomes were observed proximal to dark-grey staining Aps, which were unfused (Fig. 2Eb1-2). In osteocytes from the OVX + LG group, light grey-staining APs were observed to amass within the cytoplasm accompanied by several developed endoplasmic reticula (ER) (Fig. 2Ec1-2). These *in vivo* examinations demonstrate that LG induces osteogenic differentiation and auto-lysosomal degradation in OVX mice, and to a lesser extent, inhibits osteoclast formation in OVX mice.

LG promoted osteoblastic differentiation of MC3T3-E1 cells via enhancing auto-lysosomal degradation activity

Given that femur cellular autophagic processes are significantly influenced in OVX mice and by LG treatment *in vivo*, it was presumed that this might pertain to osteogenic differentiation and increased autophagy activity. In MTT assays, treatment with LG did not significantly alter cell viability at concentrations below 10 μM over a 48-hour time course (Fig. 3A). Thus, LG was maintained between 0.5 μM and 10 μM in all subsequent assays. In such assays, LG is deemed to promote ALP activity in a dose-dependent fashion (Fig. 3B). In comparative Western blot assays, both the 44 kDa, 30 kDa, and 15 kDa isoforms of the BMP2 osteogenic biomarker were upregulated and the levels of Beclin-1 and Lamp1 were significantly more abundant than p62 at the doses of LG applied (Fig. 3C, D).

To further explore the potential influence of LG on cellular autophagy, TEM analyses were performed (Fig. 4A). While ER, APs and mitochondria were observed in untreated control cells (Fig. 4Aa), APs, mitochondria, lysosomes, ER and well-developed Golgi bodies appeared to be more abundant within cells of the LG-treated group (Fig. 4Ab). In addition, large ALs appear to accumulate in proximity to nuclei within CQ-MC3T3-E1 cells, which might indicate an impairment in auto-lysosomal degradation function (Fig. 4Ac, B). In CQ-LG samples, ALs were visibly reduced in volume and became progressively smaller whilst Golgi bodies became seemingly more apparent (Fig. 4Ad, B). These results suggest LG exerts an influence upon intracellular auto-lysosomal degradation within MC3T3-E1 cells.

LG exerted anti-apoptosis properties within MC3T3-E1 cells

A trade-off between apoptosis and autophagy is of central importance to bone homeostasis[36] and previously reported instances of apoptosis-related proteins, notably the Bcl-2 family members,[9] prompted further investigation into the influence of LG upon autophagy-apoptosis regulation. We noted from flow cytometry assay data that there was no apparent increased apoptosis at the concentrations of LG applied (Fig. 5A–F). Furthermore, levels of Bcl-2 were significantly reduced in Western blot analyses after treatment with OIS, but more abundant in the presence of LG in a dose-dependent manner (Fig. 5G–J). In stark contrast, levels of Bax and cleaved Caspase-3 (Fig. 5H–J), were down-regulated in the presence of LG, separately. Thus, LG may prevent apoptosis of MC3T3-E1 cells.

LG partially corrected lysosomal dysfunction through promoting autophagy and inhibiting apoptosis

The correct functioning of lysosomes is critical to accurate autophagy,[37] as any dysfunction of this would inevitably promote apoptosis.[38] Here, Neutral red supravital staining was applied as a signal for lysosome activity in further quests to ascertain the influence LG on autophagy and apoptosis in osteocytes (Fig. 6). With basal numbers of hyperchromatic rufous lysosomes stained red in the vicinity of nuclei within blank- and Con-treated MC3T3-E1 cells, these significantly increased to a maximum after application of LG at the concentrations between 1.0 and 5.0 μM (Fig. 6a–f). In contrast, nuclei within CQ-treated and TS-treated MC3T3-E1 cells were encircled by transparent vacuoles and both lysosomes and ALs were stained abnormally, indicative of intracellular pH being alkaline (Fig. 6g, l). In the initial stages of staining CQ/TS-LG-treated MC3T3-E1 cells, transparent vacuoles were observed. With the increasing concentrations of LG, these gradually diminished in both number and volume, eventually being superceded by dark red-brown staining lysosomes, consistent with an acidic intracellular environment (Fig. 6h–k, m–p). These data reveal that morphologically abnormal lysosomes are

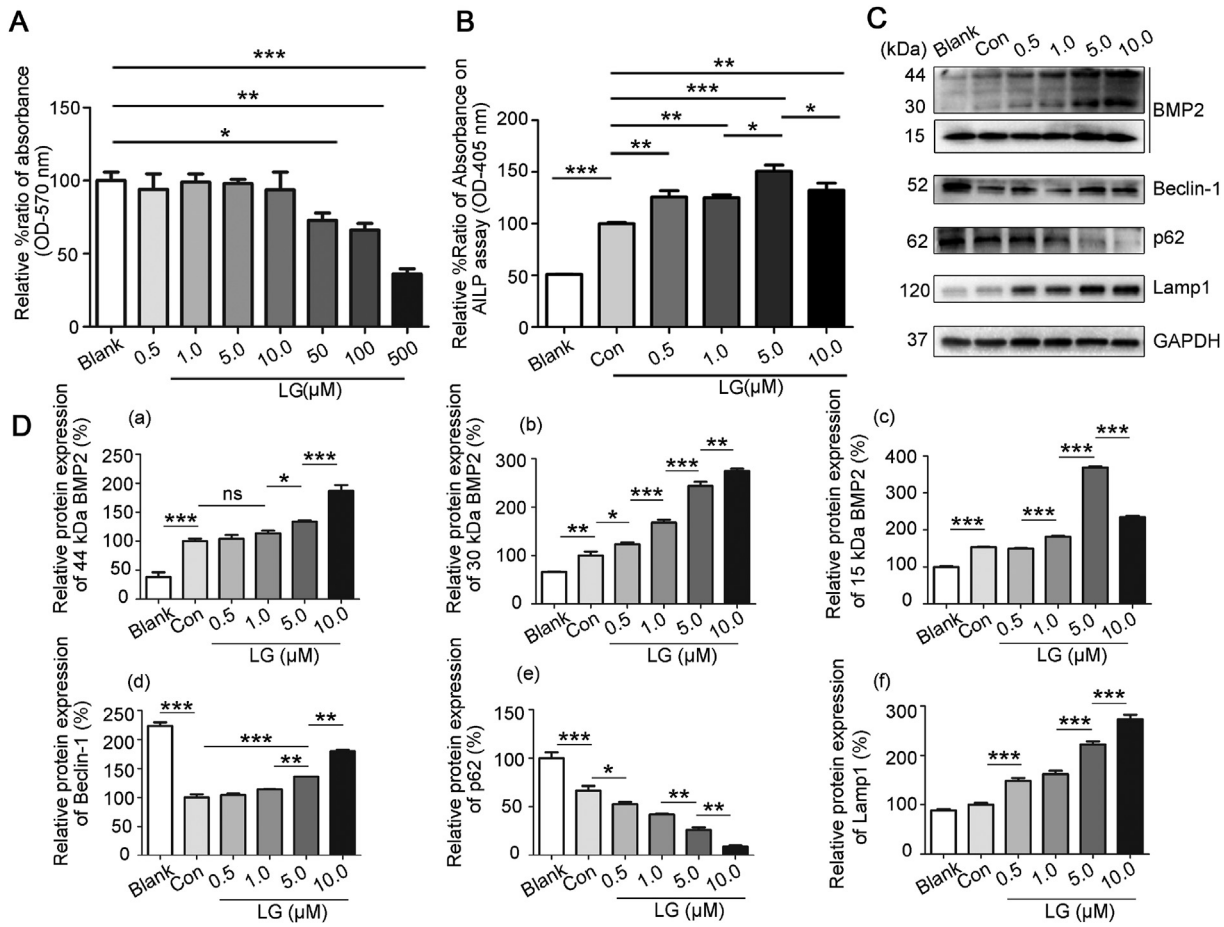

Figure 3 Effect of LG on the alkaline phosphatase (ALP) activity in MC3T3-E1 cells. Cell growth was measured by MTT assay. There was no significant difference in cell viability at LG concentrations of 0, 0.5, 1.0, 5.0, 10.0 μM (**A**). LG increased the ALP activity in a dose-dependent manner in MC3T3-E1 cells (**B**). The expression of BMP2 and autophagy-associated proteins in MC3T3-E1 cells in groups (**C**—**D**). Data are reported as the mean ± standard deviation (SD) ($n = 3$). *$P < 0.05$, **$P < 0.01$, ***$P < 0.001$ (one-way analysis of variance/Newman—Keuls test).

replaced to a limited extent within MC3T3-E1+CQ and +TS in the presence of LG.

LG partially alleviated TS-induced impairment of osteoblastic differentiation in the early stage

The effect of LG on the osteogenesis of MC3T3-E1 cells in the early stage of bone formation was investigated by ALP staining (Fig. 7A, B). These results demonstrate that LG contributes significantly to the up-regulation of ALP expression in a concentration-dependent manner (Fig. 7Aa1—f1, a2—f2, B). In the CQ-treated group, MC3T3-E1 cells developed an atypical morphology and ALP expression was significantly reduced (Fig. 7Ag1—2, B). However, no apparent difference was observed in either cellular morphology or ALP expression when cells from the CQ group and CQ-LG groups were compared (Fig. 7Ag1—k1, g2—k2, B). In the TS group, the expression of ALP was, however, appreciably lower when compared to cells within the Con group (Fig. 7Al1—2, B), and interestingly, ALP expression was increased in TS-LG cells in a dose-dependent manner (Fig. 7Al1—p1, l2—p2). Western blot analyses revealed that levels of Bax (Fig. 7C, Da), cleaved caspase-3 (Fig. 7C, Db), p62 (Fig. 7C, Dc) and Lamp1 (Fig. 7C, Dd) were significantly up-regulated in TS-treated cells and conversely, down-regulated in the TS-LG group, in an LG dose-dependent manner.

LG partially ameliorated the osteogenic differentiation impairment in the late stage caused by CQ treatment

Alizarin Red S staining was employed to ascertain whether LG could promote osteogenic differentiation of MC3T3-E1 cells in the late stage of bone formation (Fig. 8A, B). The matrix's mineralisation was more prevalent within MC3T3-E1 cells, which remained morphologically similar in the presence of LG (Fig. 8Aa1—f1, a2—f2, B). In contrast, cells from the CQ group appeared to be of a smooth dark red-staining morphology (Fig. 8Ag1—2, B) compared to Con group counterparts (Fig. 8Ab1—2, B). Furthermore, in the CQ-LG groups, augmentation of mineralised nodules was

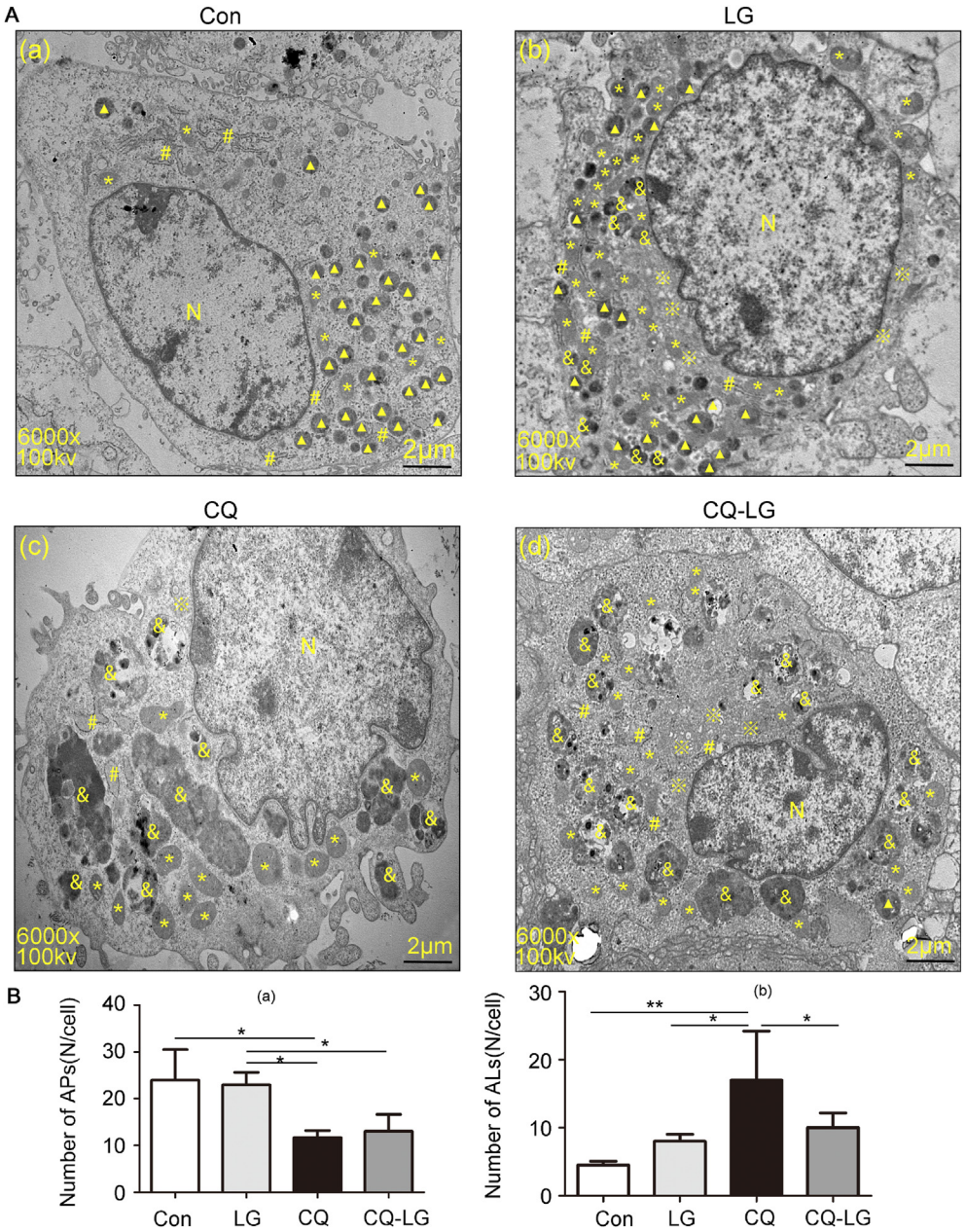

Figure 4 Effect of LG on the auto-lysosomal degradation activity in MC3T3-E1 cells. Magnification images of the ultrastructure of MC3T3-E1 cells in groups detected by TEM assay (**A**) and quantitative analysis of APs and ALs (**B**). Cell nucleus (marked as N in **Aa**–**d**), ALs (marked as & in **Aa**–**d**), mitochondria (marked as ***** in **Aa**–**d**), APs (marked as ▲ in **Aa**–**d**), developed rough endoplasmic reticula (marked as **#** in **Aa**–**d**) and Golgi apparatus (marked as ※ in **Aa**–**d**) in MC3T3-E1 cells in groups. APs: Most autophagosomes have a double membrane. Its bilayers were separated by a relatively narrower or wider electron-translucent cleft with the TEM observation. ALs: Generally, ALs had only one membrane. They contained electron-dense cytoplasmic materials and/or organelles at various stages of degradation. They were stained dark mostly in TEM samples. Mitochondria: They had a double membrane mostly. The number and distribution patterns of mitochondrial ridges are varied. Usually perpendicular to the long axis of the mitochondria, but ridges parallel to the long axis of the mitochondria can also be seen. ER: ER incuded tubulus and flat sacs and reticulates in the cytoplasm. Golgi apparatus: It could be identified as flat sacs and vesicles surrounded by a monolayer film. Most were located around the nucleus. Their sacs were not interconnected. Scale bars (E): 2 μm. Data are reported as the mean ± standard deviation (SD) ($n = 3$). $^{*}P < 0.05$, $^{**}P < 0.01$ (one-way analysis of variance/Newman–Keuls test).

apparent in an LG dose-dependent manner (Fig. 8Ah1–k1, h2–k2, B). Interestingly, bone nodules within cells from the TS group were stained light red. However, treatment with LG did not derive an increase in positive staining surface area from the TS-LG group (Fig. 8Al1–p1, l2–p2, B). Furthermore, Western blot assays revealed that the expression of p62 and Lamp1 in CQ-treated cells was significantly increased, although compared to the Con

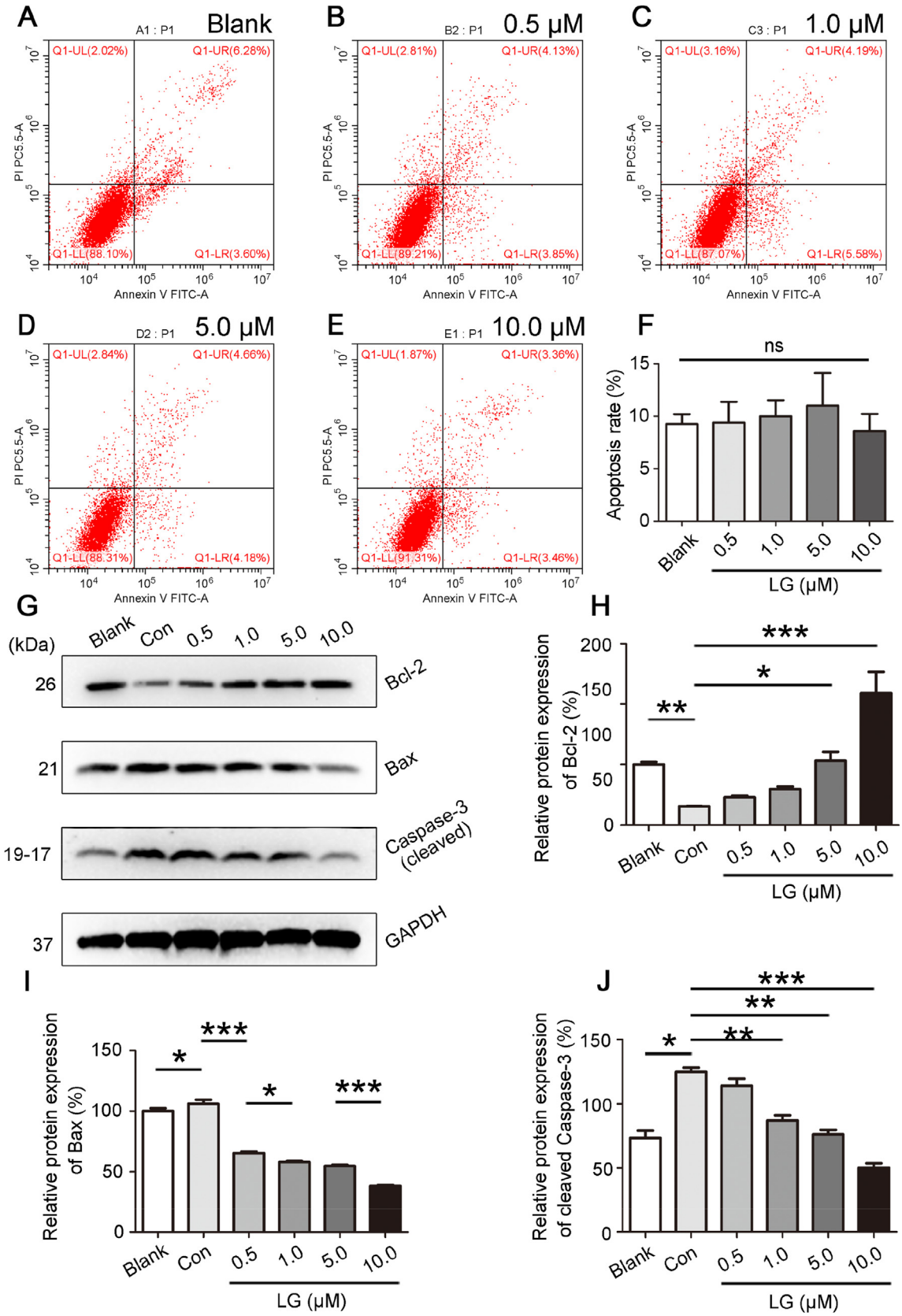

Figure 5 Effect of LG on the apoptosis in MC3T3-E1 cells. 0.5, 1.0, 5.0, 10.0 μM LG had little apoptosis-inducing effect on MC3T3-E1 cells in flow cytometry assay (**A**—**F**). The expression of apoptosis-associated proteins in MC3T3-E1 cells in groups (**G**—**J**). Data are reported as the mean ± standard deviation (SD) ($n = 3$), *$P < 0.05$, **$P < 0.01$, ***$P < 0.001$ (one-way analysis of variance/Newman—Keuls test).

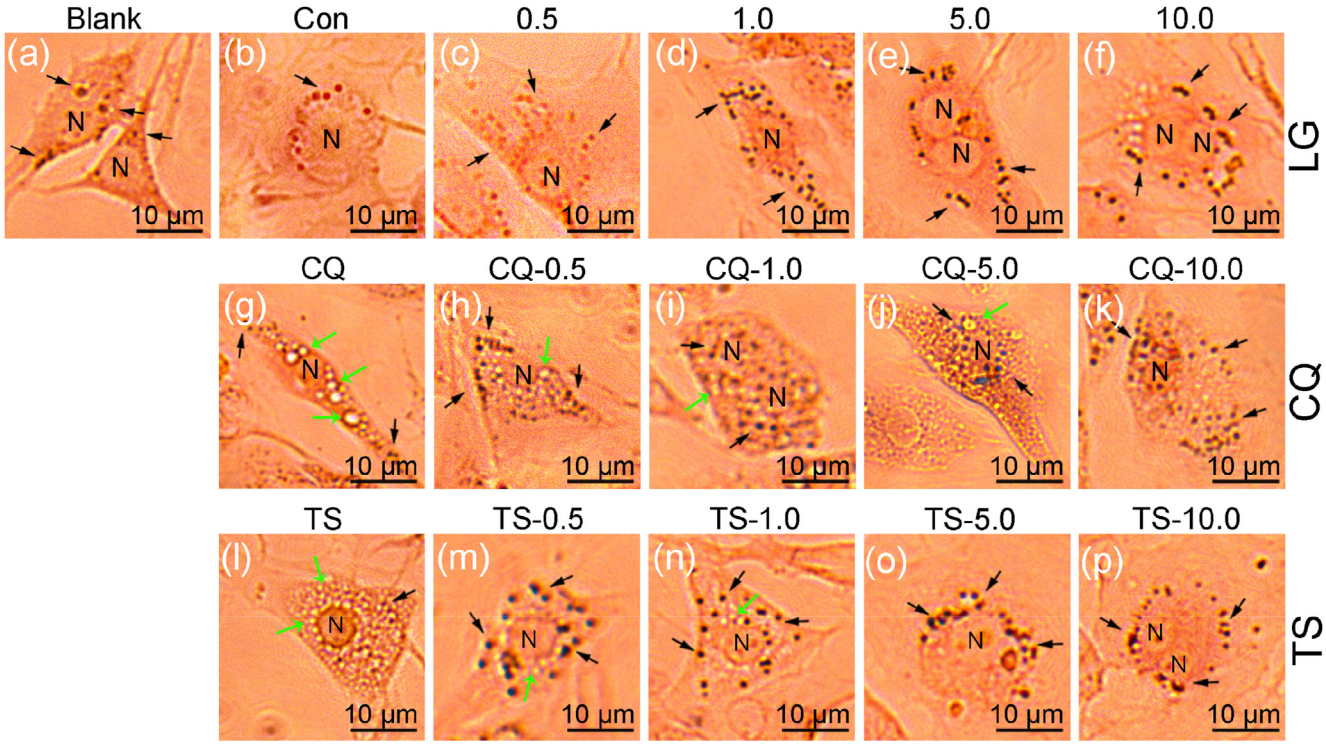

Figure 6 Effect of LG on the status of cells' lysosomes. The lysosomes of MC3T3-E1 cells in groups were stained by Neutral Red Staining ($n = 3$). Cell nucleus (marked as N in **a**–**p**), lysosomes with a pH value below 7 (black arrows in **a**–**p**) and lysosomes with a pH value of (or above) 7 (green arrows in **a**–**p**) in MC3T3-E1 cells in groups. Scale bars (B): 10 μm.

group these proteins were significantly down-regulated within cells from the CQ-LG group (Fig. 8C, Da–b). Moreover, Bcl-2 protein expression is up-regulated in a dose-dependent fashion within cells from the CQ-LG group (Fig. 8C, Dc). Overall, these results indicate that LG can over-ride the TS-induced inhibition of osteogenesis in the early stage and circumvents CQ-induced abnormal osteogenesis in the late stage *in vitro*.

Discussion

During the initial stages of the present work, an OVX mouse model was successfully established (Fig. SA, B). We demonstrated that LG improved the microstructure of trabecular bone in the distal femur from OVX mice. Additionally, LG treatment has been shown to increase the expression of osteoblastic markers, notably ALP, OPN and OC. One pertinent proviso of this phenomenon is facilitated osteoblastic differentiation. These data strongly connote that LG-promoted osteogenic differentiation over-rides a dysfunctional auto-lysosomal degradation process and obviates excessive apoptosis.

Bone accumulation derives from an equilibrium between bone deposition and degradation that favors osteoblasts.[39] It is feasible that LG could exert a dual influence *in vitro* by simultaneously promoting osteoblast differentiation and inhibiting osteoclast differentiation.[28] In the present studies, observations from IHC and TRAP staining suggests that LG treatment may bias bone microstructure formation in promoting osteoblast differentiation. Whether LG can inhibit osteoclast differentiation *in vivo* will have to await further experimentation.

Generally, osteoblasts mature into osteocytes, which have an opposing bone re-modelling function in a trade-off between bone synthesis and resorption.[40] Thus, the intracellular status of osteocytes in cancellous bone tissue *in vivo* was detected in TEM analyses. Impaired auto-lysosomal degradation was founded in the OVX group, and LG treatment significantly alleviated this. In addition, a cohort of studies within available recent literature indicates that moderate levels of autophagic activity are essential for the maintenance of first, osteoblast viability and second, homeostasis of osteoblast and osteocyte populations.[14,41] During the maturation of osteoblasts into osteocytes, effective recycling of cellular organelles occurs.[42] Under normal conditions within osteoblasts, autophagy mechanisms are inextricably linked to the resorptive activity of osteoclasts mediated by TGF-β1, IGFs and BMPs within the osteal ECM, which overarches osteoblast-related osteogenesis.[43–45] Ovariectomy or treatment with glucocorticoids can impel bone diminution through enhanced osteoclast numbers and bone resorption activities during autophagy occlusion.[46] Many studies may be shrouded in their primary focus being upon dissection of the initial stages of autophagy in osteoblasts and bone resorption within osteoclasts, which effectively overlooks the association between auto-lysosomal degradation in osteocytes and OP.

In this study, the consequences of OVX in OP progression have been exhaustively pursued and these unquestionably

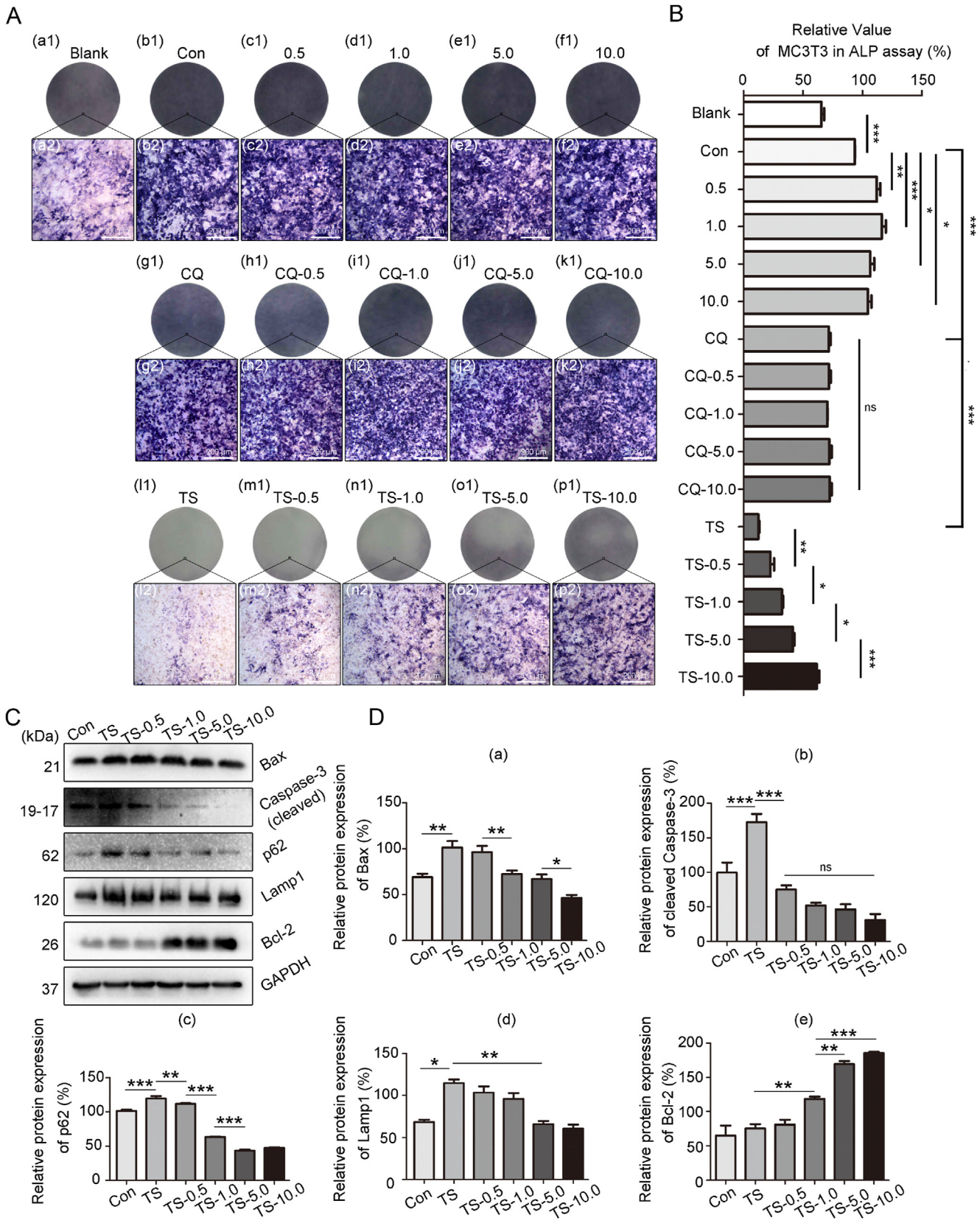

Figure 7 Effect of LG on the early stage of osteoblastic differentiation. LG increased the ALP activity in LG groups and TS-LG groups in a dose-dependent manner in MC3T3-E1 cells (**A, B**). The expression of apoptosis-associated proteins and auto-lysosomal degradation-associated proteins in MC3T3-E1 cells in groups (**C, D**). Data are reported as the mean ± standard deviation (SD) ($n = 3$), $^{*}P < 0.05$, $^{**}P < 0.01$, $^{***}P < 0.001$ (one-way analysis of variance/Newman–Keuls test).

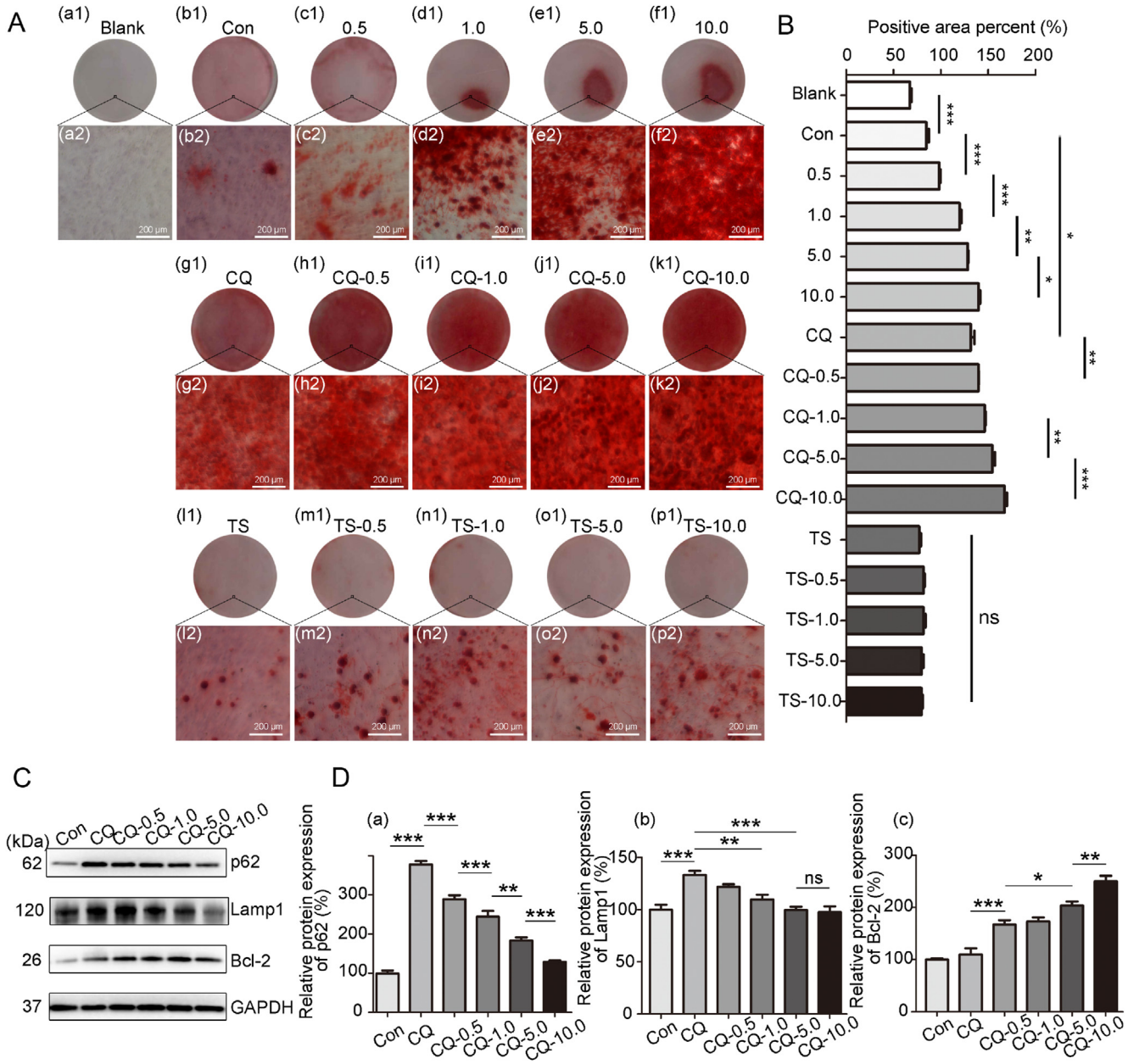

Figure 8 Effect of LG on the late stage of osteoblastic differentiation. LG increased the deposition of extracellular matrix minerals in LG groups and CQ-LG groups in a dose-dependent manner in MC3T3-E1 cells (**A, B**). The expression of auto-lysosomal degradation-associated proteins and apoptosis-associated protein Bcl-2 in MC3T3-E1 cells in groups (**C, D**). Data are reported as the mean ± standard deviation (SD) ($n = 3$), $^{*}P < 0.05$, $^{**}P < 0.01$, $^{***}P < 0.001$ (one-way analysis of variance/Newman–Keuls test).

impede intracellular AL degradation and disrupt the bioenergetic equilibrium of osteoblastic metabolism. The present study inextricably derives the LG therapeutic effect as the alleviation of auto-lysosomal degradation processes.

Western blotting analyses for autophagy-associated proteins were performed to further prospect the potential of LG in autophagy process enhancement *in vitro*. These experiments define the involvement of Beclin-1-mediated regulation of apoptosis and autophagy, specifically autophagosome-lysosome fusion and lysosomal degradation during the autophagosome-autophagic flux.[35,47] Alongside this, Lamp1, an essential lysosomal membrane component[48,49] and another membrane-associated protein, p62 (SQSTM1), should be degraded alongside damaged/dysfunctional organelles and misfolded proteins in osteoblasts.[50,51] Although levels of p62 were significantly reduced, proportions of both Lamp1 and Beclin-1 proteins increased in the presence of LG. These findings suggested that LG promotes both autophagy and lysosome production throughout osteogenesis. However, these findings contradict existing OP pathogenesis as being limited to the initial stages of autophagy as described elsewhere.[36]

Further investigations of *in vivo* auto-lysosomal degradation processes in bone cells were deemed essential and in order to visualize this intracellular phenomenon, TEM assays were performed. In contrast to the Con group, levels of APs, lysosomes, ER and well-developed Golgi bodies are elevated within an otherwise regular cytosolic topology within MC3T3-E1 cells from the LG-treated group. The endoplasmic reticula (ER) and Golgi bodies are important substrates for autophagosome formation in cells and for inhibition of ER-Golgi trafficking, autophagy may be suppressed.[52] Such notions suggest that LG may promote autophagy in MC3T3-E1 cells. Furthermore, CQ treatment may also influence auto-lysosomal degradation. This may be typified by the presence of excessive numbers of ALs, here and elsewhere.[53] In cells of the CQ-LG group, however, a resurgence of ER and Golgi bodies was accompanied by appreciably reduced levels of ALs. Comparable findings were also obtained for MC3T3-E1 cells in a novel application of Neutral red staining to assess cell viability during autophagy *in vitro*.[54] These histological observations indicate that CQ may prevent damaged organelles from being removed from cells alongside the accumulation of allotrophins within APs, a process that culminates in enlarged ALs.[52] Comparable findings were obtained in Western blot analyses in which levels of p62 and Lamp1 were found to be higher in samples from the CQ group compared to CQ-LG groups. Consequently, it is plausible that LG could overcome the disruption of autophagic degradation in the presence of CQ.

Interestingly, in studies of LG dose-responses, expression of the anti-apoptosis protein, Bcl-2[55] was significantly upregulated whilst apoptosis-promoting Bax and cleaved Caspase-3 proteins were somewhat reduced in a dose-dependent fashion. Thus, LG may prevent the formation of interactions between mitochondrial pore proteins and Bax. This would increase mitochondrial membrane permeability, which mediates inactivation of the caspase-3 pathway and precludes apoptosis.[56,57] The fact that Beclin-1 is also upregulated in the presence of LG further demonstrates its therapeutic countermand of apoptosis in bone formation.

During the induction of apoptosis there is a requirement for the presence of so-termed 'induction' proteins. In the present study, particulars of the autophagy-apoptosis mechanism within osteoblasts were investigated further to include the TS complex, which is comprised of two inductive components, the pro-inflammatory cytokine, TNF-α and the bivalent apoptosis-inducer/tumour regressor SM-164.[58] It was found that TS partially induces the production of abnormal APs and lysosomes in a manner akin to that observed in the presence of CQ. Comparable findings were also obtained for MC3T3-E1 cells stained with Neutral red. These findings consistent with the notion that LG impacts on osteogenesis may relate to impaired autophagic degradation in the presence of TS and CQ (see above). What's more, these results further demonstrate a wider influence of LG upon degradation of ALs whilst also reducing apoptosis *in vitro*.

In order to determine which stage of osteoblast differentiation is most influenced by LG, assays for ALP, a major enzyme biomarker specific to the onset of osteoblastic differentiation/maturation,[59] were performed alongside Alizarin Red S staining *in vitro*. It was found that LG promotes the onset osteogenic differentiation and findings from Western blot assays for Bax and cleaved caspase-3 suggest that LG can over-ride TS-induced suppression of ALP transcription. Along with down-regulation of Lamp1 and p62 protein expression in the TS/LG-treated sample, these findings relate to the effect of LG on ALs and lysosomes observed through Neutral red histological staining. These data clearly indicated that LG influences osteogenic differentiation within MC3T3-E1 cells during the early stage of osteoblast differentiation and offset dysfunctional AL degradation and excessive apoptosis.

The impact of LG on osteogenic differentiation during the late stage was assessed by Alizarin Red S staining indicative of bone mineralisation. Under normal conditions, the ECM secreted after the osteogenic induction allows cells to connect and subsequently aggregate. In the presence of LG, mineralisation of the matrix appeared first in high levels of cellular aggregates (Fig. 8Ad1—f1). Additionally, ECM secretions became more apparent as a gradient of increased stain intensity proportional to calcium deposition in an LG dose-dependent manner. In contrast, the ECM was stained dark red with an even and regular cell surface consistency, but cellular processes gradually disappeared within samples from the CQ group. These data indicated that MC3T3 cells pass through cellular degradation processes that culminate in cell death. This presumably involves the inhibition of intracellular auto-lysosomal degradation mechanisms coupled with increased plasma membrane permeability due to long-term CQ treatment. Furthermore, cells in the CQ-LG groups which were initially stained dark-red, appeared more intense in an LG concentration-dependent manner. It is pertinent that concentrations of between 0.5 μM and 10.0 μM LG were deemed harmless to cells as determined from survival studies in MTT and flow cytometry assays. These findings derive the notion that LG promotes calcium deposition in a dose-dependent fashion in the CQ-LG treated group prior to CQ-induced cell death of the MC3T3 cell line. Furthermore, in Western blot assays, it was found that LG could partially alleviate inhibition of auto-lysosomal degradation by countermanding CQ-mediated apoptosis.

In summation, the present *in vivo* and *in vitro* investigations clearly demonstrate LG as potential therapeutic agent for OP. These results corroborate the observations that treatment with LG can enhance osteogenic differentiation by partially over-riding dysfunction of auto-lysosomal degradation mechanisms and thereby, reduce apoptosis. These studies also provide clear definition of abnormal osteoblastic differentiation within the early stage that is caused by TS and within the late stage, as a consequence of treatment with CQ (Fig. 9). These novel approaches and timely discoveries provide new soundings for therapeutic strategies and candidate drugs for the treatment OP and other skeletal diseases.

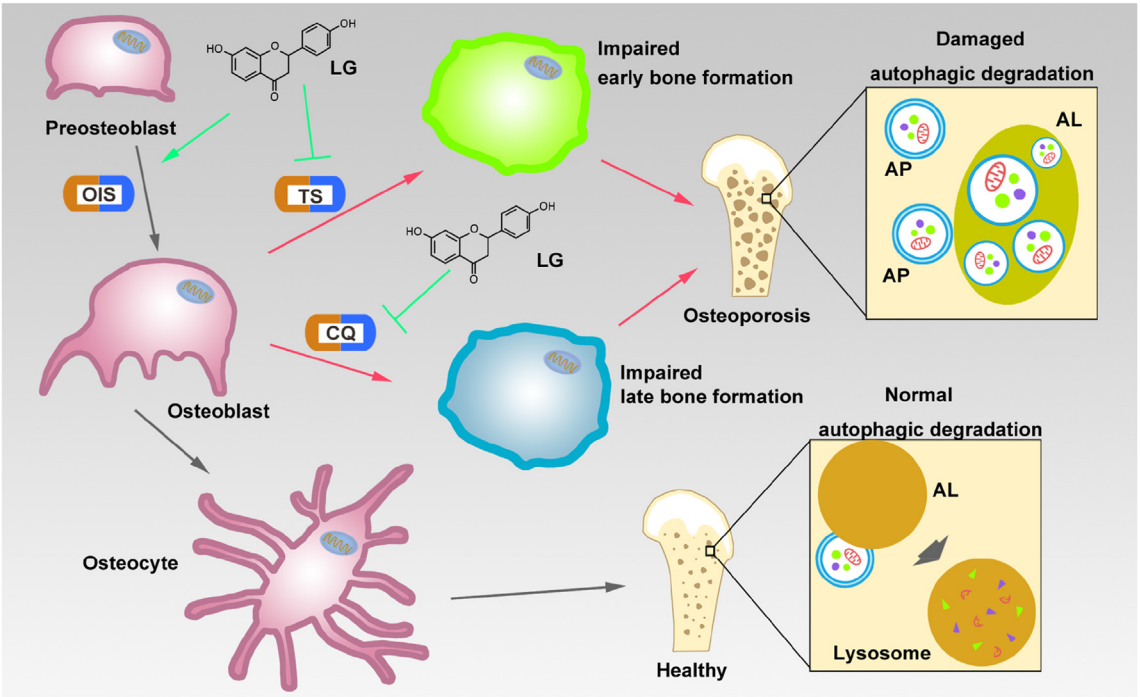

Figure 9 The underlying mechanism by which LG improves osteoporosis in the early and late stages of the osteogenesis. In physiological conditions, normal autophagic degradation maintains the process of osteogenic differentiation (presteoblasts→osteoblasts→osteocytes) and the statue of healthy bone. TS and CQ treatments damaged the early and late osteogenic differentiation, respectively, during which APs cannot be degraded in lysosomes and accumulate in ALs which resembles the impaired autophagic degradation in osteoporosis *in vivo*. To reverse this process, LG exerted protective effects in two aspects: (1) promoted the differentiation of preosteoblasts (can be induced by OIS) to osteoblasts; (2) partially corrected the dysfunctional auto-lysosomal degradation process and excessive apoptosis caused by TS and CQ treatments.

Author contributions

Yu Qiu: Conceptualization, literature search, Methodology, Software, Data curation, Writing- Original draft preparation.
Yueyang Zhao: Conceptualization, Methodology, Software, Data curation, Writing- Original draft preparation.
Zhimin Long: statistical analysis, technical support.
Aijia Song: literature search, TEM performing.
Peng Huang: literature search, TEM performing.
Kejian Wang: Software, Validation, technical support.
Ling Xu: Conceptualization, Writing- Reviewing and Editing, Funding acquisition.
David Paul Molloy: technical support, Writing- Reviewing and Editing.
Guiqiong He: Conceptualization, Methodology, Validation, Writing- Reviewing and Editing, Funding acquisition.

Conflict of interests

The authors declare no conflict of interests.

Funding

This study was supported by the National Natural Science Foundation of China (No. 81671257, 81371221, 31600825) 81671257, 81371221, 31600825) Innovation Research Group at Institutions of Higher Education in Chongqing, China (No. CXQTP19019019034) Program for Innovation Team Building at Institutions of Higher Education in Chongqing in 2016.

Acknowledgements

We thank Dr. W. Zhou (Affiliated Rehabilitation Hospital of Chongqing Medical University) for donating MC3T3-E1 cells in the experiments.

Appendix A. Supplementary data

Supplementary data to this article can be found online at https://doi.org/10.1016/j.gendis.2021.06.008.

References

1. Consensus development conference: diagnosis, prophylaxis, and treatment of osteoporosis. *Am J Med*. 1993;94(6):646—650.
2. Ensrud KE, Crandall CJ. *Osteoporosis*. *Ann Intern Med*. 2017;167(3):ITC17—ITC32.
3. Melton 3rd LJ. How many women have osteoporosis now? *J Bone Miner Res*. 1995;10(2):175—177.
4. Tabatabaei-Malazy O, Salari P, Khashayar P, et al. New horizons in treatment of osteoporosis. *Daru*. 2017;25(1):e2.

5. Black DM, Rosen CJ. Clinical practice. Postmenopausal osteoporosis. *N Engl J Med*. 2016;374(3):254—262.
6. Satué M, Arriero Mdel M, Monjo M, et al. Quercitrin and taxifolin stimulate osteoblast differentiation in MC3T3-E1 cells and inhibit osteoclastogenesis in RAW 264.7 cells. *Biochem Pharmacol*. 2013;86(10):1476—1486.
7. Moreau K, Luo S, Rubinsztein DC. Cytoprotective roles for autophagy. *Curr Opin Cell Biol*. 2010;22(2):206—211.
8. Yang Z, Klionsky DJ. Eaten alive: a history of macroautophagy. *Nat Cell Biol*. 2010;12(9):814—822.
9. Mizushima N, Levine B, Cuervo AM, et al. Autophagy fights disease through cellular self-digestion. *Nature*. 2008; 451(7182):1069—1075.
10. Mizushima N. Autophagy: process and function. *Genes Dev*. 2007;21(22):2861—2873.
11. Hocking LJ, Whitehouse C, Helfrich MH. Autophagy: a new player in skeletal maintenance? *J Bone Miner Res*. 2012;27(7): 1439—1447.
12. Wu J, Wang A, Wang X, et al. Rapamycin improves bone mass in high-turnover osteoporosis with iron accumulation through positive effects on osteogenesis and angiogenesis. *Bone*. 2019; 121:16—28.
13. Jaber FA, Khan NM, Ansari MY, et al. Autophagy plays an essential role in bone homeostasis. *J Cell Physiol*. 2019;234(8): 12105—12115.
14. Nollet M, Santucci-Darmanin S, Breuil V, et al. Autophagy in osteoblasts is involved in mineralization and bone homeostasis. *Autophagy*. 2014;10(11):1965—1977.
15. Moriishi T, Fukuyama R, Miyazaki T, et al. Overexpression of BCLXL in osteoblasts inhibits osteoblast apoptosis and increases bone volume and strength. *J Bone Miner Res*. 2016; 31(7):1366—1380.
16. Wu X, Li S, Xue P, et al. Liraglutide inhibits the apoptosis of MC3T3-E1 cells induced by serum deprivation through cAMP/PKA/β-catenin and PI3K/AKT/GSK3β signaling pathways. *Mol Cell*. 2018;41(3):234—243.
17. Maiuri MC, Zalckvar E, Kimchi A, et al. Self-eating and self-killing: crosstalk between autophagy and apoptosis. *Nat Rev Mol Cell Biol*. 2007;8(9):741—752.
18. Mialet-Perez J, Vindis C. Autophagy in health and disease: focus on the cardiovascular system. *Essays Biochem*. 2017; 61(6):721—732.
19. Cao Y, Li Q, Liu L, et al. Modafinil protects hippocampal neurons by suppressing excessive autophagy and apoptosis in mice with sleep deprivation. *Br J Pharmacol*. 2019;176(9): 1282—1297.
20. Fimia GM, Piacentini M. Regulation of autophagy in mammals and its interplay with apoptosis. *Cell Mol Life Sci*. 2010;67(10): 1581—1588.
21. Doherty J, Baehrecke EH. Life, death and autophagy. *Nat Cell Biol*. 2018;20(10):1110—1117.
22. Weinstein RS, Manolagas SC. Apoptosis and osteoporosis. *Am J Med*. 2000;108(2):153—164.
23. New SA, Robins SP, Campbell MK, et al. Dietary influences on bone mass and bone metabolism: further evidence of a positive link between fruit and vegetable consumption and bone health? *Am J Clin Nutr*. 2000;71(1):142—151.
24. Mühlbauer RC, Lozano A, Reinli A. Onion and a mixture of vegetables, salads, and herbs affect bone resorption in the rat by a mechanism independent of their base excess. *J Bone Miner Res*. 2002;17(7):1230—1236.
25. Lee JY, Lee JH, Park JH, et al. Liquiritigenin, a licorice flavonoid, helps mice resist disseminated candidiasis due to Candida albicans by Th1 immune response, whereas liquiritin, its glycoside form, does not. *Int Immunopharm*. 2009;9(5): 632—638.
26. Choi EM. Liquiritigenin isolated from Glycyrrhiza uralensis stimulates osteoblast function in osteoblastic MC3T3-E1 cells. *Int Immunopharm*. 2012;12(1):139—143.
27. Choi EM, Suh KS, Lee YS. Liquiritigenin restores osteoblast damage through regulating oxidative stress and mitochondrial dysfunction. *Phytother Res*. 2014;28(6):880—886.
28. Uchino K, Okamoto K, Sakai E, et al. Dual effects of Liquiritigenin on the proliferation of bone cells: promotion of osteoblast differentiation and inhibition of osteoclast differentiation. *Phytother Res*. 2015;29(11):1714—1721.
29. Bae GD, Park EY, Baek DJ, et al. Liquiritigenin prevents palmitate-induced beta-cell apoptosis via estrogen receptor-mediated AKT activation. *Biomed Pharmacother*. 2018;101: 348—354.
30. Yang EJ, Park GH, Song KS. Neuroprotective effects of liquiritigenin isolated from licorice roots on glutamate-induced apoptosis in hippocampal neuronal cells. *Neurotoxicology*. 2013;39:114—123.
31. From the American Association of Neurological Surgeons (AANS), American Society of Neuroradiology (ASNR), Cardiovascular and Interventional Radiology Society of Europe (CIRSE), et al. Multisociety consensus quality improvement revised consensus statement for endovascular therapy of acute ischemic stroke. *Int J Stroke*. 2018;13(6):612—632.
32. Chiu YJ, Lee CM, Lin TH, et al. Chinese herbal medicine Glycyrrhiza inflata reduces αβ aggregation and exerts neuroprotection through anti-oxidation and anti-inflammation. *Am J Chin Med*. 2018;46(7):1535—1559.
33. Du Y, Luo M, Du Y, et al. Liquiritigenin decreases αβ levels and ameliorates cognitive decline by regulating microglia M1/M2 transformation in AD mice. *Neurotox Res*. 2021;39(2):349—358.
34. Dempster DW, Compston JE, Drezner MK, et al. Standardized nomenclature, symbols, and units for bone histomorphometry: a 2012 update of the report of the ASBMR Histomorphometry Nomenclature Committee. *J Bone Miner Res*. 2013;28(1):2—17.
35. Klionsky DJ, Abdel-Aziz AK, Abdelfatah S, et al. Guidelines for the use and interpretation of assays for monitoring autophagy (4th edition). *Autophagy*. 2021;17(1):1—382.
36. Yin X, Zhou C, Li J, et al. Autophagy in bone homeostasis and the onset of osteoporosis. *Bone Res*. 2019;7:e28.
37. Myerowitz R, Puertollano R, Raben N. Impaired autophagy: the collateral damage of lysosomal storage disorders. *EBioMedicine*. 2021;63:e103166.
38. Ansari MY, Ball HC, Wase SJ, et al. Lysosomal dysfunction in osteoarthritis and aged cartilage triggers apoptosis in chondrocytes through BAX mediated release of Cytochrome c. *Osteoarthritis Cartilage*. 2021;29(1):100—112.
39. Rachner TD, Khosla S, Hofbauer LC. Osteoporosis: now and the future. *Lancet*. 2011;377(9773):1276—1287.
40. Capulli M, Paone R, Rucci N. Osteoblast and osteocyte: games without frontiers. *Arch Biochem Biophys*. 2014;561:3—12.
41. Qi M, Zhang L, Ma Y, et al. Autophagy maintains the function of bone marrow mesenchymal stem cells to prevent estrogen deficiency-induced osteoporosis. *Theranostics*. 2017;7(18): 4498—4516.
42. Dallas SL, Bonewald LF. Dynamics of the transition from osteoblast to osteocyte. *Ann N Y Acad Sci*. 2010;1192:437—443.
43. Xu X, Zheng L, Yuan Q, et al. Transforming growth factor-β in stem cells and tissue homeostasis. *Bone Res*. 2018;6:e2.
44. Qiu T, Crane JL, Xie L, et al. IGF-I induced phosphorylation of PTH receptor enhances osteoblast to osteocyte transition. *Bone Res*. 2018;6:e5.
45. Chen L, Jiang W, Huang J, et al. Insulin-like growth factor 2 (IGF-2) potentiates BMP-9-induced osteogenic differentiation and bone formation. *J Bone Miner Res*. 2010;25(11): 2447—2459.

46. Lin NY, Chen CW, Kagwiria R, et al. Inactivation of autophagy ameliorates glucocorticoid-induced and ovariectomy-induced bone loss. *Ann Rheum Dis*. 2016;75(6):1203—1210.
47. Kang R, Zeh HJ, Lotze MT, et al. The Beclin 1 network regulates autophagy and apoptosis. *Cell Death Differ*. 2011;18(4): 571—580.
48. Eskelinen EL, Tanaka Y, Saftig P. At the acidic edge: emerging functions for lysosomal membrane proteins. *Trends Cell Biol*. 2003;13(3):137—145.
49. Eskelinen EL. Roles of LAMP-1 and LAMP-2 in lysosome biogenesis and autophagy. *Mol Aspect Med*. 2006;27(5—6): 495—502.
50. Pankiv S, Clausen TH, Lamark T, et al. p62/SQSTM1 binds directly to Atg8/LC3 to facilitate degradation of ubiquitinated protein aggregates by autophagy. *J Biol Chem*. 2007;282(33): 24131—24145.
51. Moscat J, Diaz-Meco MT. p62 at the crossroads of autophagy, apoptosis, and cancer. *Cell*. 2009;137(6):1001—1004.
52. Gui X, Yang H, Li T, et al. Autophagy induction via STING trafficking is a primordial function of the cGAS pathway. *Nature*. 2019;567(7747):262—266.
53. Pasquier B. Autophagy inhibitors. *Cell Mol Life Sci*. 2016;73(5): 985—1001.
54. Gomez-Gutierrez JG, Bhutiani N, McNally MW, et al. The neutral red assay can be used to evaluate cell viability during autophagy or in an acidic microenvironment in vitro. *Biotech Histochem*. 2021;96(4):302—310.
55. Deng X, Xiao L, Lang W, et al. Novel role for JNK as a stress-activated Bcl2 kinase. *J Biol Chem*. 2001;276(26): 23681—23688.
56. Walensky LD. Targeting BAX to drug death directly. *Nat Chem Biol*. 2019;15(7):657—665.
57. Shalini S, Dorstyn L, Dawar S, et al. Old, new and emerging functions of caspases. *Cell Death Differ*. 2015;22(4):526—539.
58. Lu J, Bai L, Sun H, et al. SM-164: a novel, bivalent Smac mimetic that induces apoptosis and tumor regression by concurrent removal of the blockade of cIAP-1/2 and XIAP. *Cancer Res*. 2008;68(22):9384—9393.
59. Hong D, Chen HX, Yu HQ, et al. Morphological and proteomic analysis of early stage of osteoblast differentiation in osteoblastic progenitor cells. *Exp Cell Res*. 2010;316(14): 2291—2300.